Exact Symbol Error Probabilities for SVD Transmission of BPSK Data over Fading Channels

Lee M. Garth Peter J. Smith
Department of Electrical and Computer Engineering
University of Canterbury, Christchurch, New Zealand

Mansoor Shafi
Telecom New Zealand Limited
Wellington, New Zealand

***Abstract*— In this paper we derive a generalized method to compute the error probabilities of singular value decomposition-based receivers for a MIMO system with uncoded transmission. The method can be used for a wide class of flat fading environments, including i.i.d. and semi-correlated Rayleigh and i.i.d. Ricean channels. Although we apply the method to equal-power BPSK, it can easily be extended to higher order M-PSK and M-QAM signal constellations and adaptive "water-filling" schemes. The error probability curves derived from closed-form formulas and simulations demonstrate very close agreement. We also compare the error performances of CI, MMSE and ZF receivers with the SVD receiver.**

I. Introduction

The pioneering work of [1] has resulted in immense interest in MIMO systems. They offer the promise of large system capacities, and thus are being considered for fourth generation wireless systems. In this paper we study the error performance of certain MIMO systems and make the following contributions:

- We present a generalized method that can be used to derive the exact symbol error probability of singular value decomposition (SVD)-based MIMO receivers using uncoded transmission. We demonstrate the method for i.i.d. and semi-correlated Rayleigh and i.i.d. Ricean channels. Our results provide new insights in understanding the error performance of MIMO systems. For example, when the number of antennas is increased from two each at the transmit and receive ends to four, whilst the ergodic capacity increases, the error performance degrades. Hence, we are able to quantify the tradeoff between ergodic capacity and system outage.
- We compare the SVD receiver error performance with channel inversion (CI), minimum mean square error (MMSE) and zero forcing (ZF) receivers and show that for all types of channels and SNR the MMSE receiver outperforms the other receivers.

Finally, our analytical method for equal-power BPSK can be extended to derive exact symbol error probabilities for higher-order signal constellations (M-PSK & M-QAM) and adaptive "water-filling" schemes, but this is beyond the scope of this paper.

II. Background

Here we consider a single-user MIMO BPSK system with perfect channel state information (CSI) at both the transmitter and receiver. We model the channel using a variety of flat fading models including uncorrelated and correlated Rayleigh models and a Ricean model. For a MIMO system with n_T transmit and n_R receive antennas the received signal can be written

$$\boldsymbol{r} = \boldsymbol{H}\,\boldsymbol{s} + \boldsymbol{n}, \tag{1}$$

where $\boldsymbol{r}$ is the $n_R \times 1$ received signal vector, $\boldsymbol{s}$ is the complex $n_T \times 1$ transmitted signal vector and $\boldsymbol{H}$ is an $n_R \times n_T$ complex channel gain matrix. The AWGN vector $\boldsymbol{n}$ consists of n_R independent noise components with $\mathrm{var}(\mathrm{Re}[n_i]) = \sigma_n^2/2$.

If we have perfect CSI, we can perform a singular value decomposition of $\boldsymbol{H} = \boldsymbol{U}\boldsymbol{D}\boldsymbol{V}$, where $\boldsymbol{U}$ and $\boldsymbol{V}$ are unitary matrices and $\boldsymbol{D}$ is a diagonal matrix with entries $\sqrt{\lambda_k}$, $k = 1, \ldots, m$. Here, we denote length $m = \min(n_T, n_R)$, $n = \max(n_T, n_R)$, and the λ_k's are the distinct eigenvalues of

$$\boldsymbol{W} = \begin{cases} \boldsymbol{H}\,\boldsymbol{H}^\dagger, & \text{for } n_R \le n_T \\ \boldsymbol{H}^\dagger\,\boldsymbol{H}, & \text{for } n_T < n_R \end{cases}, \tag{2}$$

where $(\cdot)^\dagger$ denotes the conjugate transpose.

As per conventional SVD-based spatial multiplexing methods [2], [3], we precode our m-dimensional BPSK symbol vector $\boldsymbol{b}$ by multiplying it by $\boldsymbol{V}^\dagger$ and decode our received observation vector $\boldsymbol{r}$ by multiplying it by $\boldsymbol{U}^\dagger$. Defining $\boldsymbol{s} = \boldsymbol{V}^\dagger\boldsymbol{b}$, $\boldsymbol{y} = \boldsymbol{U}^\dagger\boldsymbol{r}$, and $\widetilde{\boldsymbol{n}} = \boldsymbol{U}^\dagger\boldsymbol{n}$ and transforming (1) by using the orthonormality of $\boldsymbol{U}$ and $\boldsymbol{V}$, the decoder output has the form

$$\boldsymbol{y} = \boldsymbol{D}\,\boldsymbol{b} + \widetilde{\boldsymbol{n}}. \tag{3}$$

Due to the orthonormality of $\boldsymbol{U}^\dagger$, the transformed noise vector $\widetilde{\boldsymbol{n}}$ remains white Gaussian with $\mathrm{var}(\mathrm{Re}[\widetilde{n}_i]) = \sigma_n^2/2$. Because $\boldsymbol{D}$ is diagonal, the MIMO channel (1) has been transformed into m parallel channels of the form

$$y_k = \sqrt{\lambda_k}\,b_k + \widetilde{n}_k, \quad k = 1, \ldots, m. \tag{4}$$

"Water-filling" could be performed along the parallel channels by sending different sized signal constellations down each channel. However, in this paper we only consider the equal power distribution method with identical BPSK constellations for each channel. Normalizing the transmitted BPSK symbols by n_T to keep the total transmitted signal power constant, we let $\mathrm{Prob}\left(b_k = 1/\sqrt{n_T}\right) = \mathrm{Prob}\left(b_k = -1/\sqrt{n_T}\right) = 1/2$. The optimal detector for each parallel channel is then

$$\widehat{b}_k = \mathrm{sgn}(\mathrm{Re}[y_k]). \tag{5}$$

0-7803-8938-7/05/$20.00 (C) 2005 IEEE

Since the probability of error is the same for all combinations of positive and negative binary symbols in $\boldsymbol{b}$, the probability of a MIMO symbol error for this system is

$$\begin{aligned}
P_s &= 1 - \text{Prob}\left(\widehat{b}_1, \widehat{b}_2, \ldots, \widehat{b}_m \text{ all correct}\right) \\
&= 1 - \text{Prob}\left(\sqrt{\tfrac{\lambda_1}{n_T}} + \text{Re}[\widetilde{n}_1] > 0, \ldots, \sqrt{\tfrac{\lambda_m}{n_T}} + \text{Re}[\widetilde{n}_m] > 0\right) \\
&= 1 - \text{E}\left\{\Phi\left(\tfrac{\sqrt{\lambda_1}}{\sigma}\right) \times \Phi\left(\tfrac{\sqrt{\lambda_2}}{\sigma}\right) \times \cdots \times \Phi\left(\tfrac{\sqrt{\lambda_m}}{\sigma}\right)\right\} \\
&= 1 - \int_0^\infty \cdots \int_0^\infty \prod_{i=1}^m \Phi\left(\tfrac{\sqrt{\lambda_i}}{\sigma}\right) f(\lambda_1, \ldots, \lambda_m)\, d\lambda_1 \ \ldots \ d\lambda_m \\
&= 1 - \int_{\boldsymbol{\lambda}} \prod_{i=1}^m \Phi\left(\tfrac{\sqrt{\lambda_i}}{\sigma}\right) f(\boldsymbol{\lambda})\, d\boldsymbol{\lambda}, \qquad (6)
\end{aligned}$$

where $\sigma^2 = n_T\, \sigma_n^2/2$ and $\Phi(x)$ is the cumulative distribution function of a standard Gaussian variable, i.e. $\Phi(x) = \text{Prob}(Z \le x)$ for $Z \sim N(0,1)$.

The joint density of the *unordered* eigenvalues for an i.i.d. Rayleigh fading channel is well known [4], [1] and with the constant Δ defined by $\Delta = \{\prod_{k=1}^m [(n-k)!\,(m-k)!]\}^{-1}$ is given by

$$\begin{aligned}
f_I(\boldsymbol{\lambda}) &= \frac{\Delta}{m!} \exp\left\{-\sum_{k=1}^m \lambda_k\right\} \prod_{k=1}^m \lambda_k^{n-m} \prod_{i<j} (\lambda_i - \lambda_j)^2 \\
&= \frac{\Delta}{m!} \prod_{k=1}^m \left(\lambda_k^{n-m} e^{-\lambda_k}\right) \begin{vmatrix} 1 & \ldots & 1 \\ \lambda_1 & \ldots & \lambda_m \\ \vdots & & \vdots \\ \lambda_1^{m-1} & \ldots & \lambda_m^{m-1} \end{vmatrix}^2 \\
&= \frac{\Delta}{m!} \begin{vmatrix} 1 & \ldots & 1 \\ \lambda_1 & \ldots & \lambda_m \\ \vdots & & \vdots \\ \lambda_1^{m-1} & \ldots & \lambda_m^{m-1} \end{vmatrix} \\
&\quad \times \begin{vmatrix} \lambda_1^{n-m} e^{-\lambda_1} & \ldots & \lambda_m^{n-m} e^{-\lambda_m} \\ \lambda_1^{n-m+1} e^{-\lambda_1} & \ldots & \lambda_m^{n-m+1} e^{-\lambda_m} \\ \vdots & & \vdots \\ \lambda_1^{n-1} e^{-\lambda_1} & \ldots & \lambda_m^{n-1} e^{-\lambda_m} \end{vmatrix} \\
&\triangleq \frac{C}{m!}\, \Upsilon(\boldsymbol{\lambda})\, |\Psi_{ij}(\lambda_j)|\,. \qquad (7)
\end{aligned}$$

The last representation for this density is purposely generic. With suitable definitions of C and Ψ_{ij} we are able to cast each of the channel models we consider in this general form.

As shown in [1], an alternative form of the Vandermonde determinant $\Upsilon(\boldsymbol{\lambda})$ is

$$\begin{aligned}
\Upsilon(\boldsymbol{\lambda}) &= \begin{vmatrix} 1 & \ldots & 1 \\ \vdots & & \vdots \\ \lambda_1^{m-1} & \ldots & \lambda_m^{m-1} \end{vmatrix} \\
&= \sum_\alpha (-1)^{\text{per}(\alpha)} \prod_{k=1}^m \lambda_k^{\alpha_k - 1}, \qquad (8)
\end{aligned}$$

where α is a permutation of $(1, \ldots, m)$. The summation runs over all possible permutations of $(1, \ldots, m)$, and $(-1)^{\text{per}(\alpha)}$ gives the sign of the permutation (i.e., $\text{per}(\alpha)$ represents the number of column swaps required to order $(\alpha_1, \ldots, \alpha_m)$). The term $|\Psi_{ij}(\lambda_j)|$ in (7) denotes the determinant of the $m \times m$ matrix with ij-th element $\Psi_{ij}(\lambda_j)$.

Substituting (7) and (8) into (6) gives

$$\begin{aligned}
P_s &= 1 - \frac{C}{m!} \sum_\alpha (-1)^{\text{per}(\alpha)} \\
&\qquad \times \int_{\boldsymbol{\lambda}} \prod_{j=1}^m \left\{\Phi\left(\tfrac{\sqrt{\lambda_j}}{\sigma}\right) \lambda_j^{\alpha_j - 1}\right\} |\Psi_{ij}(\lambda_j)|\, d\boldsymbol{\lambda} \\
&= 1 - \frac{C}{m!} \sum_\alpha (-1)^{\text{per}(\alpha)} \int_{\boldsymbol{\lambda}} \left|\Phi\left(\tfrac{\sqrt{\lambda_j}}{\sigma}\right) \lambda_j^{\alpha_j - 1}\, \Psi_{ij}(\lambda_j)\right| d\boldsymbol{\lambda} \\
&= 1 - \frac{C}{m!} \sum_\alpha (-1)^{\text{per}(\alpha)} \left|[\boldsymbol{g}(1, \alpha_1) \cdots \boldsymbol{g}(m, \alpha_m)]\right|. \qquad (9)
\end{aligned}$$

Here each column vector has the form $\boldsymbol{g}(j, \alpha_j) = [g_1(j, \alpha_j), \ldots, g_m(j, \alpha_j)]^T$, where

$$g_i(j, \alpha_j) = \textstyle\int_0^\infty \Phi\left(\sqrt{\lambda_j}/\sigma\right)\, \lambda_j^{\alpha_j - 1}\, \Psi_{ij}(\lambda_j)\, d\lambda_j.$$

Reordering the columns in (9) gives

$$P_s = 1 - \frac{C}{m!} \sum_\alpha \left|[\boldsymbol{g}(\alpha_1, 1) \cdots \boldsymbol{g}(\alpha_m, m)]\right|, \qquad (10)$$

since reordering the columns so $\alpha_1, \ldots, \alpha_m$ are in order yields a $(-1)^{\text{per}(\alpha)}$ factor. Fortunately, vector $\boldsymbol{g}(\alpha_j, j)$ is independent of α_j since α_j simply locates the eigenvalue which is being integrated. Hence, all determinants of the sum (10) are equal. Because there are $m!$ permutations in the sum, we finally have

$$P_s = 1 - C\, \left|[\boldsymbol{g}(1) \cdots \boldsymbol{g}(m)]\right|, \qquad (11)$$

where $\boldsymbol{g}(j) = [g_1(j), \ldots, g_m(j)]^T$ and

$$g_i(j) = \int_0^\infty \Phi\left(\tfrac{\sqrt{\lambda}}{\sigma}\right) \lambda^{j-1}\, \Psi_{ij}(\lambda)\, d\lambda. \qquad (12)$$

This is the step which makes analysis realistic as sums over $m!$ permutations are undesirable. Note that this form of solution is valid for any channel with joint eigenvalue density given by (7). Eigenvalue densities of this form include those for the i.i.d. and semi-correlated Rayleigh and i.i.d. Ricean channels.

III. I.I.D. Rayleigh Channel

As shown in (7), for the i.i.d. Rayleigh fading channel, the constant $C = \Delta$ and the function $\Psi_{ij}(\lambda_j)$ has the specific form $\lambda_j^{n-m+i-1} e^{-\lambda_j}$. Therefore, we have

$$\begin{aligned}
g_i(j) &= \int_0^\infty \Phi\left(\tfrac{\sqrt{\lambda}}{\sigma}\right) \lambda^{n-m+j+i-2} e^{-\lambda}\, d\lambda \\
&= \xi(n-m+j+i-2, \sigma). \qquad (13)
\end{aligned}$$

Using the relation $\Phi(x) = 1 - Q(x)$, where $Q(\cdot)$ is the Gaussian tail probability, we can rewrite (13) in the generic form

$$\begin{aligned}
\xi(r, \sigma) &\triangleq \int_0^\infty \Phi\left(\tfrac{\sqrt{\lambda}}{\sigma}\right) \lambda^r e^{-\lambda}\, d\lambda \\
&= r! - \int_0^\infty Q\left(\tfrac{\sqrt{\lambda}}{\sigma}\right) \lambda^r e^{-\lambda}\, d\lambda. \qquad (14)
\end{aligned}$$

But as shown in [5, p.825], the second term on the right can be simplified as

$$\int_0^\infty Q\left(\tfrac{\sqrt{\lambda}}{\sigma}\right)\lambda^r e^{-\lambda}\,d\lambda = r!\,\left\{\tfrac{1}{2}[1-\mu(\sigma)]\right\}^{r+1} \times \textstyle\sum_{k=0}^{r}\binom{r+k}{k}\left\{\tfrac{1}{2}[1+\mu(\sigma)]\right\}^k, \quad (15)$$

where

$$\mu(\sigma) = \sqrt{\tfrac{1}{1+2\sigma^2}}. \quad (16)$$

(Even though the noise variance σ^2 appears by itself, $\mu(\sigma)$ is dimensionless due to the implicit ratio of σ^2 with the unit signal power.) Hence, for the i.i.d. Rayleigh channel P_s can be computed in closed form using (11) in conjunction with (13) – (16).

Figure 1 shows our calculated and simulated symbol error probabilities versus SNR for (2,2), (2,4), (4,2) and (4,4) MIMO systems. Our calculations line up very well with our simulations which are based on 500,000 Monte Carlo runs.

We also compare our results for the SVD method with the channel inversion (CI) method [6], which requires CSI at the transmitter, as well as the classical MMSE and ZF methods, which require CSI only at the receiver. The CI method works for $n_T \geq n_R$ and involves sending $\widetilde{\boldsymbol{s}} = \boldsymbol{H}^\dagger(\boldsymbol{H}\boldsymbol{H}^\dagger)^{-1}\boldsymbol{b}$. Unlike [6], to keep the average transmit power equal to one, we need to normalize by the rms power of $\widetilde{\boldsymbol{s}}$. But, we can write

$$\begin{aligned}\mathrm{E}\{\|\boldsymbol{H}^\dagger(\boldsymbol{H}\boldsymbol{H}^\dagger)^{-1}\boldsymbol{b}\|^2\} &= \mathrm{Tr}[\boldsymbol{H}^\dagger(\boldsymbol{H}\boldsymbol{H}^\dagger)^{-1}\mathrm{E}\{\boldsymbol{b}\,\boldsymbol{b}^\dagger\}(\boldsymbol{H}\boldsymbol{H}^\dagger)^{-\dagger}\boldsymbol{H}] \\ &= \tfrac{1}{n_T}\mathrm{Tr}[(\boldsymbol{H}\boldsymbol{H}^\dagger)^{-1}] = \tfrac{1}{n_T}\textstyle\sum_{k=1}^{n_R}\tfrac{1}{\lambda_k}. \end{aligned} \quad (17)$$

Therefore, at the receiver we observe

$$\boldsymbol{y}^{\mathrm{CI}} = \left(\tfrac{1}{n_T}\textstyle\sum_{k=1}^{n_R}\tfrac{1}{\lambda_k}\right)^{-1/2}\boldsymbol{b} + \boldsymbol{n} \quad (18)$$

and decode

$$\widehat{\boldsymbol{b}}^{\mathrm{CI}} = \mathrm{sgn}\left(\mathrm{Re}\left[\boldsymbol{y}^{\mathrm{CI}}\right]\right). \quad (19)$$

The classical MMSE and ZF methods are decoded using

$$\begin{aligned}\widehat{\boldsymbol{b}}^{\mathrm{MMSE}} &= \mathrm{sgn}\{\mathrm{Re}[(\sigma_n^2\boldsymbol{I} + \boldsymbol{H}^\dagger\boldsymbol{H})^{-1}\boldsymbol{H}^\dagger(\boldsymbol{H}\,\boldsymbol{b}+\boldsymbol{n})]\} \\ \widehat{\boldsymbol{b}}^{\mathrm{ZF}} &= \mathrm{sgn}\{\mathrm{Re}[(\boldsymbol{H}^\dagger\boldsymbol{H})^{-1}\boldsymbol{H}^\dagger(\boldsymbol{H}\,\boldsymbol{b}+\boldsymbol{n})]\}. \end{aligned} \quad (20)$$

The ZF method requires that $n_T \leq n_R$.

Figure 2 shows our simulated symbol error probabilities versus SNR for all four MIMO methods using the (2,2) and (4,4) antenna configurations. We see that for both configurations, the MMSE method outperforms the other methods, given equal signal power allocation among the parallel channels for the SVD and CI methods and among the transmitting antennas for the MMSE and ZF methods. The other three methods have very similar performances. The MMSE method utilizes both the channel and noise statistics, whereas the other three methods only use the channel statistics. Unfortunately, with the symbol error probability dominated by the worst eigen-channels, the considered equal-power version of the SVD method does not exploit the better eigen-channels. The advantage of the SVD method lies in the ability to "water-fill" the eigen-channels with different-sized signal constellations, increasing the capacity of the MIMO system for a given symbol error probability. Finally, note that the diversity gains of the four methods are the same.

IV. Semi-Correlated Rayleigh Channel

In [7], we considered the "semi-correlated" Rayleigh channel model, where the transceiver end which only has m antennas experiences spatial correlation. For example, if $n_R \leq n_T$, then the receiving antennas are spatially correlated and the columns of $\boldsymbol{H}$ are i.i.d., each with covariance matrix $\boldsymbol{\Gamma}$. Likewise, if $n_R > n_T$, then the transmitting antennas are spatially correlated and the columns of $\boldsymbol{H}^\dagger$ have covariance $\boldsymbol{\Gamma}$. As shown in [8], the distinct unordered eigenvalues $\boldsymbol{\lambda}$ then have joint density

$$f_{SC}(\boldsymbol{\lambda}) = \frac{\Delta}{m!}\,\frac{\prod_{\ell=1}^{m}[(\ell-1)!]}{|\Xi_{ij}(\gamma_j)|}\,\Upsilon(\boldsymbol{\lambda})\,|\Psi_{ij}(\lambda_j)|\,, \quad (21)$$

where $\Xi_{ij}(\gamma_j) = (-1)^{i-1}\,\gamma_j^{n-i+1}$, $\Psi_{ij}(\lambda_j) = \lambda_j^{n-m}\,e^{-\lambda_j/\gamma_i}$ and $\boldsymbol{\gamma} = [\gamma_1\ \cdots\ \gamma_m]^T$ is a vector containing the eigenvalues of $\boldsymbol{\Gamma}$. Thus, error probability P_s has the form (11) with

$$C = [\textstyle\prod_{k=1}^{m}[(n-k)!]\ |\Xi_{ij}(\gamma_j)|]^{-1}$$

and

$$\begin{aligned} g_i(j) &= \int_0^\infty \Phi\left(\tfrac{\sqrt{\lambda}}{\sigma}\right)\lambda^{n-m+j-1}e^{-\lambda/\gamma_i}\,d\lambda \\ &= \gamma_i^{n-m+j}\,\xi(n-m+j-1, \sigma/\sqrt{\gamma_i}), \end{aligned} \quad (22)$$

which can be evaluated using (14) – (16).

Figure 3 shows our calculated and simulated symbol error probabilities versus SNR for (2,2), (2,4), (4,2) and (4,4) MIMO systems. We have calculated P_s for a $\lambda/2$-spaced transmitter or receiver (depending on which has fewer antennas) with high spatial correlation $\boldsymbol{\Gamma}$ defined for the generalized ITU pedestrian environment A for a macrocell with Laplacian power azimuth spectrum and a 5^o angle spread [9]. Again, our calculations line up very well with our simulations which are based on 500,000 Monte Carlo runs. Note that the large correlation produces a larger eigenvalue spread with smaller $\lambda_{\min}$ than the i.i.d. Rayleigh case. Since $\lambda_{\min}$ dominates P_s, the semi-correlated case performances are inferior to those of the i.i.d. case.

Again, for this semi-correlated Rayleigh case we compare the SVD method with the CI, MMSE and ZF methods. Figure 4 shows our P_s versus SNR for all four MIMO methods using the (2,2) and (4,4) antenna configurations. Again, due to the lack of "water-filling" in the SVD method and the intelligent use of the noise statistics, the MMSE method outperforms the other methods with the other three methods having very similar performances.

V. I.I.D. RICEAN CHANNEL

We finally compute the probability of MIMO symbol error for an i.i.d. Ricean fading channel. As discussed in [10], [11], the Ricean channel matrix $\boldsymbol{H}$ has the form

$$\boldsymbol{H} = a\,\boldsymbol{H}^{\rm sp} + b\,\boldsymbol{H}^{\rm sc} \tag{23}$$

where the specular and scattered components of $\boldsymbol{H}$ are denoted by superscripts. Matrix $\boldsymbol{H}^{\rm sp}$ is deterministic with unit magnitude elements, and the entries of $\boldsymbol{H}^{\rm sc}$ are independent, zero mean, unit variance, complex Gaussians. The parameters a and b satisfy $a^2 + b^2 = 1$ so that the SNR is not scaled by the channel. In standard models [10] the specular matrix is defined as:

$$\boldsymbol{H}^{\rm sp} = \boldsymbol{a}(\theta_r)\,\boldsymbol{a}(\theta_t)^T, \tag{24}$$

where $\boldsymbol{a}(\theta_r)$ and $\boldsymbol{a}(\theta_t)$ are the specular array responses at the receiver and transmitter. If a k-element array is linear, the response is $\boldsymbol{a}(\theta) = \left[1 \;\; e^{j2\pi d\cos(\theta)} \;\; \cdots \;\; e^{j2\pi d(k-1)\cos(\theta)}\right]^T$, where θ is the angle of arrival or departure of the specular component, and d is the antenna spacing in wavelengths. This form gives the specular matrix a rank of one. We will use this model in our numerical results, although our analysis holds for more general forms of $\boldsymbol{H}^{\rm sp}$. The strength of the LOS component is measured using the K-factor, $K = 10\,\log_{10}\left(a^2/b^2\right)$ dB.

To simplify the notation, we let $(w_1, w_2, \ldots, w_m)$ be the eigenvalues of $\widetilde{\boldsymbol{W}} = \boldsymbol{W}/b^2$. Thus, we have $w_k = \lambda_k/b^2$. We also need to define the associated LOS version of $\boldsymbol{W}$ in (2) as the matrix $\boldsymbol{M}$, where

$$\boldsymbol{M} = \begin{cases} \frac{a^2}{b^2}\,\boldsymbol{H}^{\rm sp}\,\boldsymbol{H}^{\rm sp\dagger}, & \text{for} \;\; n_R \le n_T \\ \frac{a^2}{b^2}\,\boldsymbol{H}^{\rm sp\dagger}\,\boldsymbol{H}^{\rm sp}, & \text{for} \;\; n_T < n_R \end{cases}. \tag{25}$$

The eigenvalues of $\boldsymbol{M}$ are denoted by $(f_1, f_2, \ldots, f_m)$. In the rank one standard model for $\boldsymbol{M}$, these eigenvalues are given by: $f_1 = \frac{a^2}{b^2}\,m\,n$ and $f_2 = f_3 = \ldots = f_m = 0$.

As shown in [12], the distinct unordered eigenvalues $\boldsymbol{w}$ (with corresponding distinct eigenvalues $\boldsymbol{f}$) have joint density

$$f_R(\boldsymbol{w}) = \frac{1}{m!\;|\Xi_{ij}(f_j)|}\,\Upsilon(\boldsymbol{w})\;|\Psi_{ij}(w_j)|\,, \tag{26}$$

where $\Psi_{ij}(w_j) = w_j^{(n-m)/2}\,e^{-(f_i+w_j)}\,I_{n-m}\left(2\sqrt{f_i\,w_j}\right)$, $\Xi_{ij}(f_j) = f_j^{(n-m)/2+i-1}$ and $I_\ell(\cdot)$ is a modified Bessel function. Thus, the error probability P_s has the form (11) with $C = |\Xi_{ij}(f_j)|^{-1}$ and

$$g_i(j) = \int_0^\infty \Phi\left(\tfrac{\sqrt{w}}{\sigma/b}\right) w^{(n-m)/2+j-1} e^{-(f_i+w)} \times I_{n-m}\left(2\sqrt{f_i\,w}\right)\,dw. \tag{27}$$

We are unaware of an analytical solution to this integral. Nevertheless, numerical integration can be performed to evaluate P_s for the Ricean channel case.

For the special case of a rank one specular matrix the numerator and denominator of (26) are zero for $m > 2$. To cope with this situation, we need to compute the following limit

$$\lim_{f_2,f_3,\ldots,f_m\to 0} \left|I_{n-m}\left(2\sqrt{f_i\,w_j}\right)\right| \Big/ \left|f_j^{(n-m)/2+i-1}\right|. \tag{28}$$

In Appendix I we derive this limit and hence compute the joint density of the unordered eigenvalues as

$$f_{R1}(\boldsymbol{w}) = \frac{(-1)^{m-1}\,f_1^{-(n+m)/2+1}\,e^{-f_1}}{m!\,\prod_{k=2}^m\left[(n-k)!\,(m-k)!\right]} \times \sum_\alpha (-1)^{{\rm per}(\alpha)}\,|\boldsymbol{r}_{\alpha_1}\;\boldsymbol{r}_{\alpha_2}\;\cdots\;\boldsymbol{r}_{\alpha_m}|\,. \tag{29}$$

In (29) the vectors $\boldsymbol{r}_{\alpha_1}$,$\boldsymbol{r}_{\alpha_2}$,...,$\boldsymbol{r}_{\alpha_m}$ are defined by

$$\boldsymbol{r}_{\alpha_j} = w_j^{n-m+\alpha_j-1}e^{-w_j} \times \left[w_j^{-(n-m)/2}I_{n-m}\left(2\sqrt{f_1\,w_j}\right)\;1\;w_j\;\cdots\;w_j^{m-2}\right]^T. \tag{30}$$

Following the same methodology as in (9) – (11), we are able to remove the summation of permutations in (29). For the rank one case, this leads to a P_s of the form (11) with

$$C = \frac{(-1)^{m-1}\,f_1^{-(n+m)/2+1}}{\prod_{k=2}^m\left[(n-k)!\,(m-k)!\right]}.$$

The first row of vector $\boldsymbol{g}(j)$, $g_1(j)$, is of the form shown in (27), and the other rows ($2 \le i \le m$) have elements of the form

$$g_i(j) = \int_0^\infty \Phi\left(\tfrac{\sqrt{w}}{\sigma/b}\right) w^{n-m+j+i-3}e^{-w}\,dw = \xi(n-m+j+i-3, \sigma/b). \tag{31}$$

Figure 5 shows our calculated and simulated P_s versus SNR for (2,2), (2,4), (4,2) and (4,4) MIMO systems. We have calculated the symbol error probabilities for the rank one Ricean channel with fixed angles $\theta_t = 20^o$ and $\theta_r = 35^o$, $d = 4$, and $K = 10$ dB. Here the trial parameters were selected to verify our analysis rather than to model a particular array environment. An antenna spacing of $d = 4$ wavelengths would correspond to a base station. Again, our calculations line up very well with our simulations which are based on 500,000 Monte Carlo runs. The simulated values and theoretical curves differ slightly for the (4,4) case at large SNRs due to instability of the numerical integral (27). Relative to the i.i.d. Rayleigh case, the line of sight component in the Ricean case produces a larger eigenvalue spread with smaller $\lambda_{\min}$, particularly for large m. Since $\lambda_{\min}$ dominates P_s, the Ricean case performances are inferior to those of the i.i.d. Rayleigh case.

Figure 6 shows our simulated symbol error probabilities versus SNR for the SVD, CI, MMSE and ZF methods using the (2,2) and (4,4) antenna configurations. Again, the MMSE method outperforms the other methods with the other three methods having very similar performances.

VI. Conclusion

In this paper we derive exact symbol error probabilities for SVD-based MIMO receivers and also compare their simulated performance with CI, MMSE and ZF receivers. The symbol error probabilities for the SVD-based MIMO receivers provide new insights. Whilst the capacity of MIMO systems increase with antenna numbers, the error performance degrades. This suggests that capacity increases and error performance need to be carefully considered. Finally, to take full advantage of the CSI information at the transmitter, the analysis of the SVD method should be extended to higher-order signal constellations (M-PSK & M-QAM) and adaptive "water-filling" schemes.

Appendix I
Derivation of Ricean Eigenvalue Density for Unit Rank Specular Matrix

Multiplying density (26) by $m!$, the density for the *ordered* eigenvalues w for a Ricean channel can be rewritten as

$$f_{\widetilde{R}}(\boldsymbol{w}) = \exp\left\{-\textstyle\sum_{i=1}^{m} f_i + w_i\right\} \textstyle\sum_{\alpha} (-1)^{\mathrm{per}(\alpha)} \prod_{k=1}^{m} w_k^{\alpha_k - 1} \times \prod_{\ell=1}^{m} w_\ell^{(n-m)/2} \frac{\left| f_i^{-(n-m)/2} I_{n-m}\left(2\sqrt{f_i\, w_j}\right)\right|}{\left|f_j^{i-1}\right|}. \quad (32)$$

The ratio of determinants in (32) is written as

$$\left|\boldsymbol{\eta}(f_1)\ \boldsymbol{\eta}(f_2)\ \cdots\ \boldsymbol{\eta}(f_m)\right| \Big/ \left|\boldsymbol{v}(f_1)\ \boldsymbol{v}(f_2)\ \cdots\ \boldsymbol{v}(f_m)\right| \quad (33)$$

where $\boldsymbol{\eta}(f_j) = [\eta_1(f_j)\ \eta_2(f_j)\ \cdots\ \eta_m(f_j)]^T$, $\boldsymbol{v}(f_j) = \left[1\ f_j\ \cdots\ f_j^{m-1}\right]^T$ and

$$\eta_i(f_j) = f_j^{-(n-m)/2}\, I_{n-m}\left(2\sqrt{f_j\, w_i}\right). \quad (34)$$

Both the numerator and denominator become zero in (33) for the case $f_1 > 0$, $f_2 = f_3 = \cdots = f_m = 0$. Hence we require a limiting version of (33) as $f_2, f_3, \ldots, f_m \to 0$. (Note that the exponential function of the f_i's in (32) can be handled separately since it goes to 1 in the limit.) This is evaluated by repeated use of Cauchy's mean value theorem giving

$$\lim_{f_2, f_3, \ldots, f_m \to 0} \left|\boldsymbol{\eta}(f_1)\ \cdots\ \boldsymbol{\eta}(f_m)\right| \Big/ \left|\boldsymbol{v}(f_1)\ \cdots\ \boldsymbol{v}(f_m)\right| = \frac{\left|\boldsymbol{\eta}(f_1)\ \boldsymbol{\eta}(0)\ \boldsymbol{\eta}^{(1)}(0)\ \cdots\ \boldsymbol{\eta}^{(m-2)}(0)\right|}{\left|\boldsymbol{v}(f_1)\ \boldsymbol{v}(0)\ \boldsymbol{v}^{(1)}(0)\ \cdots\ \boldsymbol{v}^{(m-2)}(0)\right|} \quad (35)$$

where $\boldsymbol{\eta}^{(k)}(0)$ and $\boldsymbol{v}^{(k)}(0)$ represent the k^{th} derivatives of $\boldsymbol{\eta}$ and $\boldsymbol{v}$ at zero. The derivatives of Bessel functions are well known [13], and so the derivatives in (35) are obtained by known results. Some straightforward algebra shows

$$\left|\boldsymbol{v}(f_1)\ \boldsymbol{v}(0)\ \cdots\ \boldsymbol{v}^{(m-2)}(0)\right| = (-1)^{m-1}\, f_1^{m-1} \prod_{k=1}^{m-2} k! \quad (36)$$

and

$$\eta_i^{(k)}(0) = w_i^{(n-m)/2+k}/(n-m+k)!. \quad (37)$$

Taking the limit of the exponential function of the f_i's and substituting (35) and (36) into (32) gives

$$f_{R1}(\boldsymbol{w}) = e^{-f_1} \frac{\left|\boldsymbol{\eta}(f_1)\ \boldsymbol{\eta}(0)\ \cdots\ \boldsymbol{\eta}^{(m-2)}(0)\right|}{\left[(-1)^{m-1}\, f_1^{m-1} \prod_{k=1}^{m-2} k!\right]} \times \sum_{\alpha} (-1)^{\mathrm{per}(\alpha)} \left[\prod_{k=1}^{m} w_k^{(n-m)/2+\alpha_k-1}\, e^{-w_k}\right]. \quad (38)$$

Moving all the terms containing $w_1, w_2, \ldots, w_m$ into the determinant of (38), we finally have

$$f_{R1}(\boldsymbol{w}) = \frac{(-1)^{m-1}\, f_1^{-(n-m)/2+1}\, e^{-f_1}}{\prod_{k=2}^{m} [(n-k)!\,(m-k)!]} \times \textstyle\sum_{\alpha} (-1)^{\mathrm{per}(\alpha)} \left|\boldsymbol{r}_{\alpha_1}\ \boldsymbol{r}_{\alpha_2}\ \cdots\ \boldsymbol{r}_{\alpha_m}\right| \quad (39)$$

where

$$\boldsymbol{r}_{\alpha_j} = w_j^{n-m+\alpha_j-1}\, e^{-w_j} \times \left[w_j^{-(n-m)/2} I_{n-m}\left(2\sqrt{f_1\, w_j}\right)\ 1\ w_j\ \cdots\ w_j^{m-2}\right]^T. \quad (40)$$

Note that the form of (39) is similar to (26) but simpler since only the first elements of the vectors $\boldsymbol{r}_1, \boldsymbol{r}_2, \ldots, \boldsymbol{r}_m$ contain Bessel functions.

References

[1] I. E. Telatar, "Capacity of multi-antenna Gaussian channels," *European Trans. on Telecomm. Related Technol.*, vol. 10, pp. 585–595, Nov.-Dec. 1999.

[2] G. G. Raleigh and J. M. Cioffi, "Spatio-temporal coding for wireless communication," *IEEE Trans. Commun.*, vol. 46, no. 3, pp. 357–366, Mar. 1998.

[3] G. Lebrun, T. Ying, and M. Faulkner, "MIMO transmission over a time-varying channel using SVD," in *Proc. 2002 IEEE Global Telecommunications Conf.*, Taipei, Taiwan, Nov. 17-21, 2002, pp. 414–418.

[4] A. T. James, "Distributions of matrix variates and latent roots derived from normal samples," *Ann. Math. Statist.*, vol. 35, no. 1, pp. 475–501, 1964.

[5] J. G. Proakis, *Digital Communications*, 4th ed. New York: McGraw-Hill, 2001.

[6] T. Haustein, C. von Helmolt, E. Jorswieck, V. Jungnickel, and V. Pohl, "Performance of MIMO systems with channel inversion," in *Proc. 55th IEEE Vehicular Technology Conf., VTC Spring 2002*, Birmingham, Alabama, May 6-9, 2002, pp. 35–39.

[7] P. J. Smith, L. M. Garth, and S. Loyka, "Exact capacity distributions for MIMO systems with small numbers of antennas," *IEEE Commun. Lett.*, vol. 7, no. 10, pp. 481–483, Oct. 2003.

[8] M. Chiani, M. Z. Win, and A. Zanella, "On the capacity of spatially correlated MIMO Rayleigh-fading channels," *IEEE Trans. Inform. Theory*, vol. 49, no. 10, pp. 2363–2371, Oct. 2003.

[9] 3GPP, "Initial channel models for MIMO," TSGR1#21(01)0902, Turin, Italy, Aug. 27-31, 2001.

[10] F. R. Farrokhi, G. J. Foschini, A. Lozano, and R. Valenzuela, "Link-optimal space-time processing with multiple transmit and receive antennas," *IEEE Commun. Lett.*, vol. 5, no. 3, pp. 85–87, Mar. 2001.

[11] P. J. Smith and L. M. Garth, "Exact capacity distributions for dual MIMO systems in Ricean fading," *IEEE Commun. Lett.*, vol. 8, no. 1, pp. 18–20, Jan. 2004.

[12] ——, "Distribution and characteristic functions of correlated complex Wishart matrices," submitted to *J. Multivariate Anal.*, Feb. 2004.

[13] I. S. Gradshteyn and I. M. Ryzhik, *Table of Integrals, Series, and Products*, 6th ed. San Diego: Academic Press, 2000.

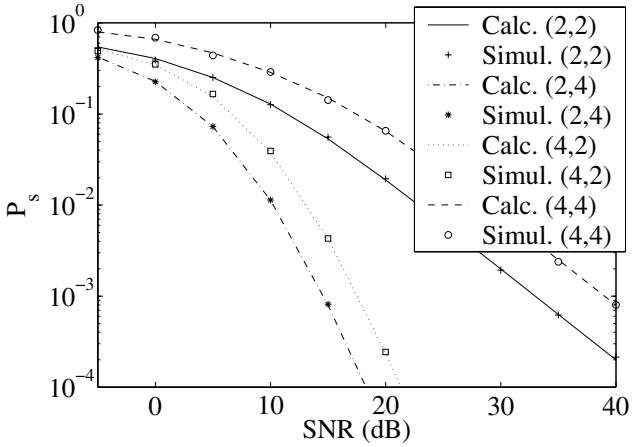

Fig. 1. SVD Symbol Error Probabilities for I.i.d. Rayleigh Case

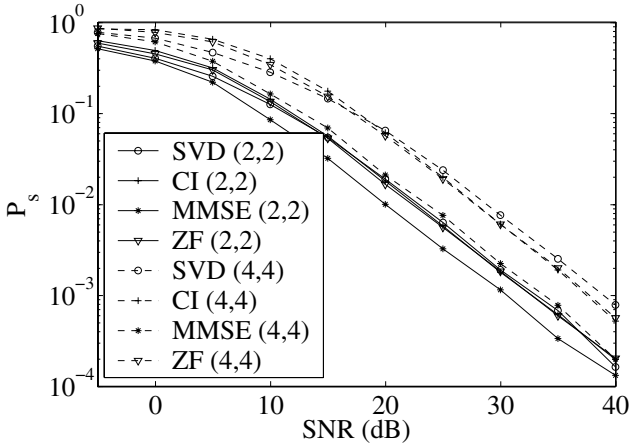

Fig. 2. Simulated Symbol Error Probabilities for I.i.d. Rayleigh Case

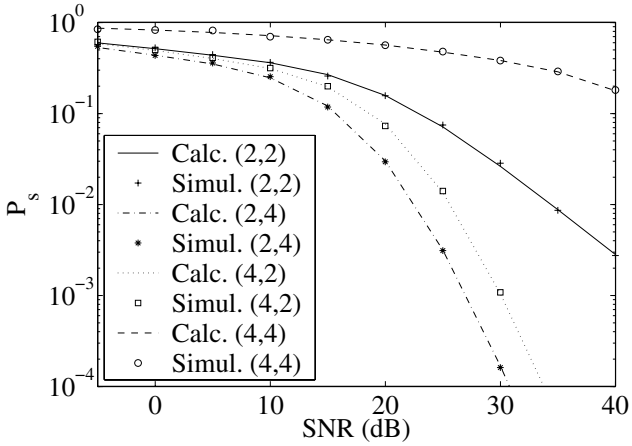

Fig. 3. Symbol Error Probabilities for Semi-Correlated Rayleigh Case

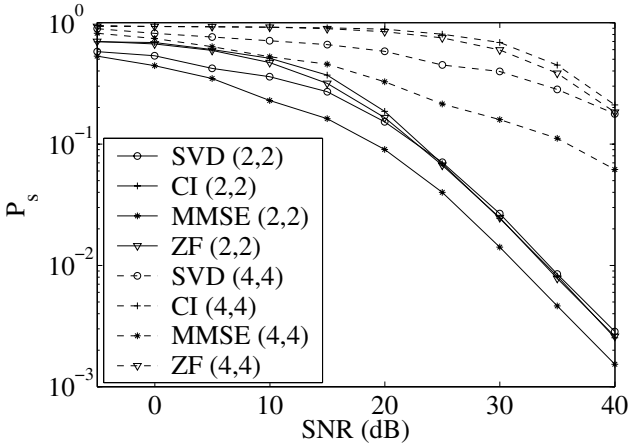

Fig. 4. Simulated Symbol Error Probabilities for Semi-Correlated Rayleigh Case

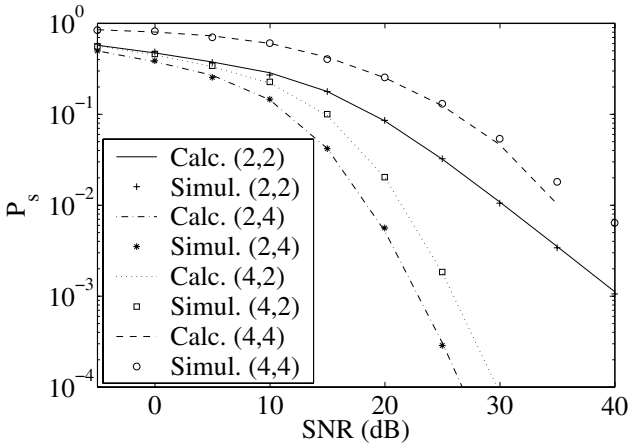

Fig. 5. Symbol Error Probabilities for Rank 1 Ricean Case

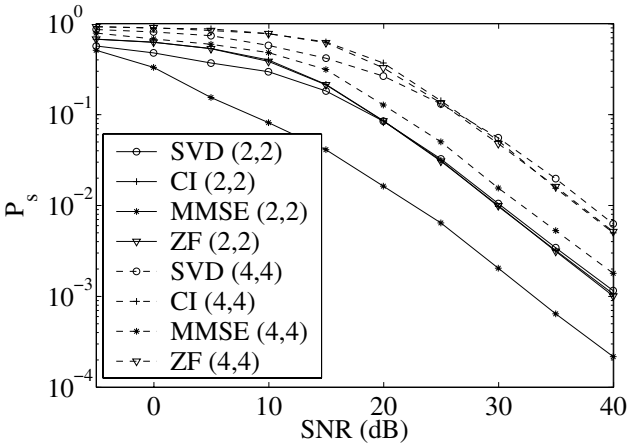

Fig. 6. Simulated Symbol Error Probabilities for Rank 1 Ricean Case